

Vibrational and elastic effects of point defects in silicon

Stewart J. Clark and Graeme J. Ackland

Department of Physics, The University of Edinburgh, JCMB, The Kings Buildings, Edinburgh EH9 3JZ, Scotland, United Kingdom

(Received 10 February 1993)

We calculate the free energies and normal modes associated with point defects in silicon. The dynamical matrices of a large relaxed supercell of perfect silicon and supercells containing defects are calculated. Diagonalization gives all the vibrational frequencies, and localized defect modes are found from the eigenvectors. The elastic effect of the defects is found by a method involving inversion of the dynamical matrices. The free energy and vibrational entropy of the defects are found by standard statistical techniques.

I. INTRODUCTION

Calculations of vibrational frequencies within perfect crystals is a relatively straightforward process.¹ The periodicity of the lattice reduces the size of the computation to diagonalizations of relatively small dynamical matrices, which are easily achieved on any small computer. When a defect is introduced into a crystal, the periodicity is lost. Therefore the symmetry properties used to reduce the size of a calculation can no longer be used. To model a defect, a supercell containing a large number of atoms can be used to reduce the finite size effects that could be caused by periodic boundary conditions used in conventional lattice dynamics of perfect crystals. In most cases this leads to a prohibitively large calculation.

There are several methods by which we can calculate vibrational frequencies in crystals containing defects. Since thermodynamic properties depend only on the sum of the eigenfrequencies, they can be obtained simply from the determinant of the dynamical matrix. This is relatively simple to calculate² and was originally done several years ago. To obtain all of the eigenfrequencies is more demanding, but was made possible by a method using Green's functions.^{3,4} In this method a cell is constructed containing the defect. An inner region around the defect is found where there is a significant difference between its matrix of force constants and that of a perfect lattice. This relies on being able to identify such a region and so is applicable only to point defects.

Another method is by direct calculation.⁵⁻⁷ A large supercell containing the defect is relaxed into its ground state. The large dynamical matrix is calculated and diagonalized. Periodic boundary conditions are used which allow more general calculations than the Green's function method since linear and planar defects can be simulated. If a modern parallel or vector computer is used for the diagonalization, the running time is no longer a significant factor, and so this method is the one which we use here.

In this paper, we present the results of several calculations. First, the 0 K configurations of various defect configurations are determined by atomistic relaxation using an empirical potential which has previously been shown to give good results on the energetics of both bulk silicon

and silicon clusters.⁸ We use the Parrinello-Rahman Lagrangian to allow the shape and size of the box to change so that no external stresses act on the supercell. The relaxed positions of the atoms and the second derivative of the potential are then used to calculate the dynamical matrices for the supercells. Diagonalization gives the vibrational frequencies and their corresponding eigenvectors. A search through the eigenvectors enables us to identify localized modes caused by the defects. A method involving inversion of the dynamical matrix is then used to calculate the elastic coefficients of both the perfect and defected crystals.

From these vibrational frequencies we calculate the change in vibrational entropy, free energy, and ionic vibrational energy induced by the defects. This is done by standard statistical methods.

We use both 216 and 512 atoms in simulations of the perfect crystal with plus and minus one atom for the interstitials and vacancy, respectively. This allows us to compare any changes in elastic properties or energetics of the crystal with changes in defect concentration and to examine the importance of finite size effects on formation energies. This involves diagonalization and inversion of up to 1539×1539 real dense symmetric matrices. We have therefore written code to carry out the entire calculation on the massively parallel Connection Machine CM200 containing 16 384 processors at the Edinburgh Parallel Computing Centre.

In Sec. II we describe the silicon model which we will use and the potential and molecular dynamics simulation used to relax the supercell. The methods by which we calculate and diagonalize the dynamical matrix are shown in Sec. III. The phonon density of states curves for various defects are also calculated and localized modes caused by the defects are found. In Sec. IV, the calculations of the elastic coefficients are described. Thermal vibrational properties are calculated in Sec. V by statistical methods.

II. MOLECULAR DYNAMICS SIMULATION

It is well known that a simple pair potential is unable to stabilize the open diamond structure of silicon, where

the lattice becomes unstable with respect to close-packed structures. There have been many attempts in recent years to formulate silicon potentials which are able to model such diverse physical properties as phase changes, defect motion and configuration, surfaces, amorphous structures, etc. One of the most commonly used potentials is that of Stillinger and Weber (SW).⁹ In the development of this potential, two conditions were adopted: first, the diamond structure is the most stable at low pressures, and secondly, the melting point and the liquid structure inferred by molecular dynamics simulations are in good agreement with experiment. The drawbacks with this potential, however, are that it contains nine fitted parameters and also a three-body term which proves cumbersome to implement. It also predicts that the diamond structure is the stable structure at all pressures.¹⁰ The present study is concerned with point defects within a silicon diamond lattice. A recent comparative study of silicon empirical interatomic potentials¹¹ concluded that none of the interatomic potentials considered appear to be superior to any of the others, each with its strengths and limitations. None were found to be totally transferable, most being able to reproduce the properties that they were fitted to, but often performing quite badly on other aspects. We therefore consider it necessary to use a potential that is able to reproduce structural properties of solid states of silicon rather than those of a solid-liquid phase transition. The potential that we have used, described below, is able to accurately describe the structure of small silicon clusters,⁸ whereas, for example, the SW potential tends to overestimate the bond length in such cases.¹¹ It has also been successfully used to calculate various structural and thermodynamic properties of the complex tetrahedrally bonded ST12 and BC8 structures in silicon^{12,13} where large amounts of distortion to bond length and bond angle occur. This type of distortion and rebonding is extremely relevant to the present study. We therefore feel that, although other potentials have greater merit in other applications, the potential presented in Ref. 14 is well suited to describing the structural and energetic properties of point defects in silicon.

This simple model based on localized electrons in covalent bonds not only reproduces the phase diagram and various defect configurations, but also reduces to a simple form.^{14,8} Each atom interacts with all other atoms with a pairwise potential. It is also bonded covalently to four of its closest neighbors. These bonds repel each other through a pairwise bond-bond potential, which is represented mathematically as a repulsion between the six possible pairs of first nearest neighbors. The form of the potential for the i th atom is

$$\Phi_i = \frac{1}{2} \sum_{j=1}^N A \exp(-\alpha r_{ij}) - \frac{1}{2} \sum_{k=1}^4 B r \exp(-\beta r_{ik}) + \sum_{k=1}^3 \sum_{l=k+1}^4 C [\cos(\omega r_{lk}) + \frac{1}{3}]^2. \quad (1)$$

The i and j subscripts run over the entire crystal, while the l and k subscripts run over the four atoms to which the central atom i is bonded.

The first term is a repulsive term in which each atom is affected by every other atom. It is short ranged and can be associated with the overlap of the ionic cores. The second term represents the four covalent bonds that an atom has to its nearest neighbors and the final term is the repulsion arising from increased overlap between the electrons in neighboring bonding orbitals of these four bonds. The value of ω is set such that this final term in the potential is zero if the two bonds are at the tetrahedral angle and at the relaxed length. This term is similar in form to that used in the SW potential.

The parameters are fitted to the diamond bond length, bulk modulus, lattice parameter, and energetics of small silicon clusters.⁸ The parameters used in this work are as follows: $A = 208\,442.8$, $B = 16.635\,88$, $\alpha = 5.673\,585$, $\beta = 1.144\,811$, $C = 1.00$, and $\omega = 0.497\,668\,7$. The units are Å and eV.

A bonding arrangement has to be found to minimize the energy of defects with this potential. For the interstitial atoms, the additional atom is placed into a perfect lattice close to the particular interstitial site to be examined. A search through the most probable bonding configurations for one where each atom has exactly four bonds, all bond lengths are less than a given maximum, and there are no threefold rings is performed. Note that bonding to an atom's four nearest neighbors is not always a correct bonding arrangement. This is because in that scheme if an atom i has a neighbor j , then it does not necessarily follow that i is a neighbor of j .

For a given bonding arrangement the energy minimum is located using a conjugate gradients routine starting from a configuration in which all atoms are given a small random displacement to break all symmetries. To check the stability of such an arrangement, a simulation comprised of a few time steps of molecular dynamics is performed and a further search for bonding configurations performed, followed by another conjugate gradients minimization of any such new configuration. The temperature in the molecular dynamics (MD) is kept low so that the interstitial configuration remains in a local minimum of energy, otherwise it could be possible for it to transform into a lower energy interstitial configuration. The procedure for the vacancy is slightly simpler: an atom is removed from the perfect lattice and the two pairs of dangling bonds allowed to join, thus keeping all atoms fourfold coordinated. Conjugate gradients then moves the atomic configuration into its lowest energy state. This iterative procedure finds the relaxed lattice structure and most probable bonding configuration and it is that structure which is used for the lattice dynamics calculation.

Using the molecular dynamics code MOLDY,¹⁵ we have performed simulations on the perfect crystal and also cells containing a vacancy and a hexagonal and tetrahedral self-interstitial.¹⁶ This code uses the Parrinello-Rahman¹⁷ method to perform constant (zero) stress molecular dynamics within a supercell with periodic boundary conditions. The bond search mechanism described above allows for changes in the bonding topology and hence for migration. We used a short time step of 1.0 fs which, combined with the Gear predictor-corrector algorithm used in the MD, meant that the integration

of the equations of motion was sufficiently accurate that although no thermostat was used, there was no drift of temperature during the simulations. The supercells used for the perfect crystal contain 216 and 512 atoms, with plus and minus one atom for the interstitials and vacancies, respectively. We found that the defect formation energies and volumes differ slightly between the two sizes of simulation, therefore a larger cell containing 1000 atoms for the perfect crystal was also used to check that the defects are sufficiently well isolated in the 512 atom cell.

These defect formation volumes and energies are shown in Table I. We find that the formation energies and volumes are similar for the two larger simulations showing that the defects are isolated for the 512 atom sized simulation. For this reason, we perform the vibrational calculations on the 512 atom supercells only. The results of the defect formation energies are in agreement with other empirical results¹⁸ in that the tetrahedral interstitial is energetically more favorable than the hexagonal interstitial by more than 1.5 eV, and *ab initio* calculations,¹⁹ showing that the tetrahedral self-interstitial has a lower formation energy (but still slightly higher in energy than we predict), although the result is highly dependent on the choice of basis set. However, the *ab initio* calculation differs numerically from the covalent bond model result for the vacancy formation energy, getting 4.4 eV for the unrelaxed cell, reducing to 3.6 eV after symmetric relaxation. The authors express some doubt as to the accuracy of this calculation due to the importance of the long range response to the Jahn-Teller distortion which they were not able to calculate purely by *ab initio* techniques. This is effectively a finite size effect and in this context we note the strong dependence on system size exhibited in Table I. We also note that the normal correlation between low formation volume and low formation energy is observed in all cases.

III. THE DYNAMICAL MATRIX

We have written a new parallelized code for performing lattice dynamics calculations on large cells using the CM200 computer. In describing it, we will use the following scheme for describing the positions of atoms within the crystal. The vectors \mathbf{a}_1 , \mathbf{a}_2 , and \mathbf{a}_3 define the shape of the primitive unit cell, forming a parallelepiped. The equilibrium position of the l th unit cell

TABLE I. The defect formation energies (in eV) and formation volumes (in \AA^3) are shown as the system size is changed. Systems I, II, and III are for 216, 512, and 1000 atoms, respectively, with plus and minus one atom for the interstitial and vacancies in the supercell. The first three columns show the energies; the second three show the volumes.

	Energy			Volume		
	I	II	III	I	II	III
Hexagonal	4.20	4.56	4.56	-5.91	-6.17	-6.18
Tetrahedral	2.52	2.53	2.53	-4.82	-4.86	-4.86
Vacancy	2.82	2.15	2.14	15.24	16.16	16.17

is given by $\mathbf{r}_l = l_1\mathbf{a}_1 + l_2\mathbf{a}_2 + l_3\mathbf{a}_3$ where l_1 , l_2 , and l_3 are integers. Each unit cell contains N atoms labeled by $k = 1, \dots, N$ hence the equilibrium position of an atom lk is $\mathbf{r}_{lk} = \mathbf{r}_l + \mathbf{r}_k$ with respect to the origin of the unit cell which contains the atom. Vibrations occur when the atoms are displaced from their equilibrium position. We allow the atoms to move by an amount $\mathbf{u}_{lk} = (u_{x_{lk}}, u_{y_{lk}}, u_{z_{lk}})$ so that the actual position of an atom is $\mathbf{R}_{lk} = \mathbf{r}_{lk} + \mathbf{u}_{lk}$.

Using similar notation to that of the original paper of Born and Huang²⁰ we show the method by which we calculate the dynamical matrix. If we let μ and ν run over the coordinate axes x , y , and z then the standard method uses the following dynamical matrix:

$$D_{\mu\nu}(\mathbf{q}_{kk'}) = \frac{1}{m} \sum_{l'l'} \Phi_{\mu\nu}(\mathbf{q}_{kk'}) \exp\{i\mathbf{q} \cdot [\mathbf{r}_{l'l'} - \mathbf{r}_{lk}]\}, \quad (2)$$

where

$$\Phi_{\mu\nu}(\mathbf{q}_{kk'}) = \left[\frac{\partial^2 \Phi}{\partial u_{\mu}(\mathbf{q}_{kk'}) \partial u_{\nu}(\mathbf{q}_{kk'})} \right]_0, \quad (\mathbf{q}_{kk'}) \neq (\mathbf{q}_{k'l'}) \quad (3)$$

(the 0 subscript indicates that the second derivative is evaluated at the positions determined previously by atomistic relaxation), and

$$\Phi_{\mu\nu}(\mathbf{q}_{kk'}) = - \sum_{(\mathbf{q}_{k'l'}) \neq (\mathbf{q}_{kk'})} \Phi_{\mu\nu}(\mathbf{q}_{k'l'}). \quad (4)$$

We will be looking at defects in the crystal which will remove the periodicity from the structure. Therefore the entire supercell can be described by $l = (0, 0, 0)$ only, and $k = 1, \dots, N$ for N atoms in the simulation. To make a comparison we will treat the perfect crystal in the same way. We treat the perfect lattice as one superlattice, which therefore has a very small Brillouin zone. This allows us to sample only at $\mathbf{q}=\mathbf{0}$ which means that $D_{\mu\nu}(\mathbf{q}_{kk'})$ is a real symmetric matrix. This ranges over the same reciprocal space points allowed by that of a fully symmetrized calculation with 64 unit cells. Thus, in effect, we are calculating the phonon frequencies of higher valued wave vectors relative to the standard diamond cell but without diagonalization of complex matrices. We are then able to calculate densities of states and the displacements associated with each normal mode, but unable to associate a given phonon with its wave vector relative to the standard unit cell. In the case of a defected lattice, the Brillouin zone is also so small that sampling of wave vectors other than $\mathbf{q}=\mathbf{0}$ is unnecessary.

The l subscripts can be dropped and setting $\mathbf{q}=\mathbf{0}$, we define our dynamical matrix as

$$D_{\mu\nu}(\mathbf{q}_{kk'}) = \frac{1}{m} \Phi_{\mu\nu_{kk'}}, \quad (5)$$

where the matrix of partial second derivatives is now

$$\Phi_{\mu\nu_{kk'}} = \left[\frac{\partial^2 \Phi}{\partial u_{\mu k} \partial u_{\nu k'}} \right]_0, \quad k \neq k', \quad (6)$$

with a similar expression for $k = k'$ from Eq. (4). By removing the sum over unit cells and carrying out the calculation as if there is no symmetry within the super-

cell (which is true in the case of crystals containing defects), we are mapping the phonon frequencies which have higher wave vectors in the standard Brillouin zone onto $\mathbf{q}=0$ relative to the larger cell.

The parallelization strategy is straightforward, with the elements of the dynamical matrix spread across processors. This data-driven parallelization is an inevitable consequence of the single instruction multiple data (SIMD) architecture of this machine.

The calculations were carried out on a silicon crystal containing 512 atoms in the supercell for the perfect lattice. We also performed calculations on crystals containing interstitial atoms at the hexagonal and tetrahedral sites and on a crystal containing a vacancy. Point defects are well described by the covalent bond charge potential, and the validity of using it to calculate phonon spectra and thermal properties is established here and also in Ref. 12.

Similar phonon density of states curves were found for the 216 and 512 atom simulations which gives us confidence that our unit cell is large enough that the $\mathbf{q}=0$ sampling is sufficient. Figure 1 shows plots of density of states of phonon frequency for the larger simulations. The shapes of the curves are similar to that of experiment²¹ although we find that the covalent bond charge potential gives the frequencies slightly lower. The perfect crystal has a phonon frequency cutoff of 11.75 THz and large narrow peaks at the lower frequencies. It can be seen that the defects cause all the peaks to broaden, especially at the higher frequencies. There are additional high frequency modes which are associated with the defects. These have frequencies above the cutoff for the perfect crystal and, as we shall see, are localized near the defect.

The eigenvector corresponding to a particular frequency gives the directions and relative amplitudes that each of the atoms in the supercell move under excitation of that mode.²² Localized modes are found by searching through the normalized eigenvectors for large displacements of any individual atom. In the cases of the interstitials, the localized mode with the largest element from the matrix of normalized eigenvectors corresponds to the interstitial atom itself. Figures 2(b) and 2(c) show the atoms around the interstitial and the directions and relative amplitudes in which they move under excitation of this mode. The perfect crystal is found to have no such localized modes. For the vacancy, Fig. 2(a), the atoms close to the defect are found to have large vibrational amplitudes in the high frequency modes while the other atoms in the supercell are almost stationary. The localized modes shown in the figure correspond to the eigenvectors with the largest single element. We find that this is also the eigenvector associated with the highest frequency (13.2 THz for the hexagonal interstitial and 13.5 THz for the tetrahedral). Each eigenvector is normalized to unity (i.e., sum of squares of the coefficients of the vector is one). The vibrational energy of the localized modes is thus concentrated in a single atom. For the hexagonal interstitial the fraction of the vibrational energy localized in this atom is 0.481, while for the tetrahedral interstitial it is 0.499. This is an order of magnitude greater than

that of the largest normalized element of any eigenvector for the perfect crystal. The vacancy shows similar characteristics, with the localized modes having the highest frequencies, although the majority of the vibrational energy is associated with four atoms adjacent to the vacant site.

In conclusion, we find that the general shape of the phonon density of states is similar to that of experiment. The low frequency modes have a higher density than

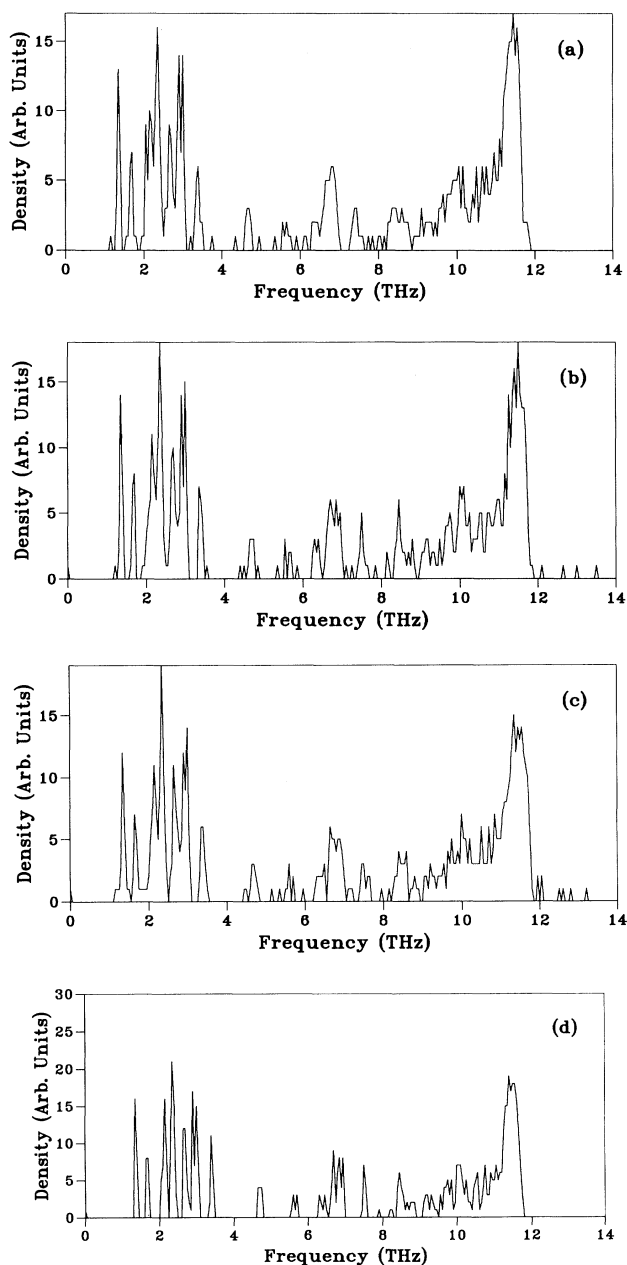


FIG. 1. Density of states plots of vibrational frequencies for the perfect and defected silicon crystals. The density is in arbitrary units. (a) is for the vacancy, (b) the tetrahedral interstitial, (c) the hexagonal interstitial, and (d) is the perfect crystal.

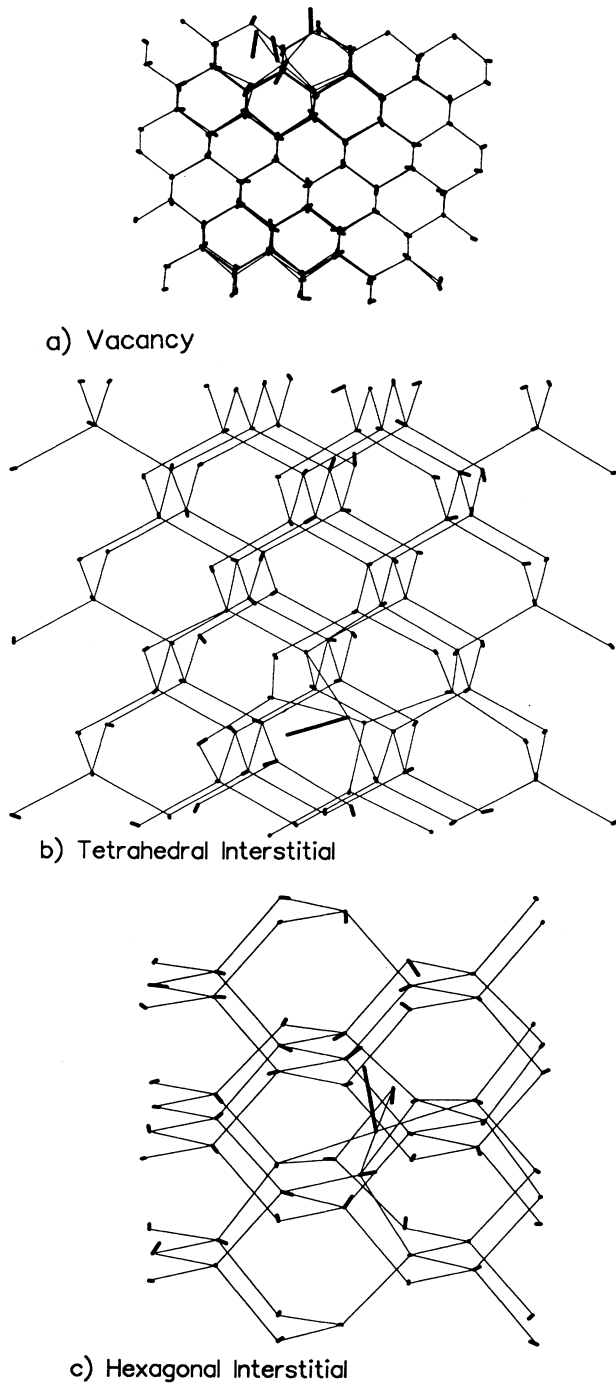


FIG. 2. Line drawings of the silicon crystals showing the localized modes. The bold lines at each atomic site show the direction and relative magnitudes of the vibrational mode under consideration. (a) shows the vacancy where the positions of the atoms surrounding the defect can be seen to relax to reduce the vacancy formation volume. There are four atoms vibrating with large amplitude for this localized mode surrounding the vacant site at the top of the diagram. (b) shows the tetrahedral interstitial and (c) the hexagonal interstitial where the single localized vibration of the interstitial atoms are clearly seen, with very little motion of the surrounding atoms.

that found experimentally, but these frequencies are in good agreement. From examination of eigenvectors of the low frequency modes it is found that these are bond-bending modes and are therefore extremely sensitive to the C parameter in the potential, but note that the same potential is being used to give the structural energies as well as phonon frequencies. There is no reason to expect that the frequencies arising from distortions in bond angle described by the simple parametrization of the covalent bond charge potential should be related to the energies associated with bond distortion. We predict a cutoff frequency of phonon modes smaller than that of experiment, but other Keating-like potentials²³ not fitted to the phonon dispersion curves often overestimate or underestimate the TO band, for example, the SW potential overestimates these frequencies by approximately 3 THz.²⁹

IV. ELASTIC CONSTANTS

There are several ways of calculating the elastic constants of a material from knowledge of the interaction potential. They can be found either from gathering statistics from long MD calculations using the fluctuation formula method,²⁵ or directly from inversion of the matrix of elastic coefficients which can be easily calculated from an empirical potential. The advantage of using the MD method is that the elastic constants can be calculated at temperature and other thermodynamic averages can be calculated simultaneously. Obviously, inverting a $3N \times 3N$ matrix at every time step in the simulation of temperature is computationally prohibitive. But our calculations are carried out at 0 K, therefore making the latter method more effective since the dynamical matrix has already been calculated.

A full derivation of the calculation of the elastic coefficients can be found in Ref. 24. We will give here the final results for a crystal containing many atoms in a single primitive unit cell. The elastic coefficients can be calculated directly from $\Phi_{\mu\nu kk'}$, as follows. We allow α , β , γ , λ , μ , and ν to run over the coordinate axes x , y , and z . Then define

$$C_{\alpha\beta}^0(kk') = \Phi_{\alpha\beta kk'}, \quad (7a)$$

$$C_{\alpha\beta,\gamma}^1(kk') = -2\pi\Phi_{\alpha\beta kk'}\Delta\gamma_{kk'}, \quad (7b)$$

$$C_{\alpha\beta,\gamma\lambda}^2(kk') = -4\pi^2\Phi_{\alpha\beta kk'}\Delta\gamma_{kk'}\Delta\lambda_{kk'}. \quad (7c)$$

There will be three modes that have zero frequency due to the three translational degrees of freedom of the entire crystal. Therefore $C_{\alpha\beta}^0(kk')$ will have linearly dependent rows and columns and hence be a singular matrix. We introduce the $(3N-3) \times (3N-3)$ matrix Γ^{3N-3} to be the inverse of $C_{\alpha\beta}^0(kk')$ ($k, k' = 2, 3, \dots, N$), and for convenience of calculation define

$$\Gamma_{\alpha\beta}(kk') = \begin{cases} \Gamma^{3N-3}(kk'), & k, k' \neq 0 \\ 0 & \text{otherwise.} \end{cases} \quad (8)$$

For convenience, we remove $k = 1$ rows and columns from the dynamical matrix for the inversion. The choice of k is arbitrary and therefore can be taken to be $k = 1$ without loss of generality.

TABLE II. Elastic coefficients in $\text{eV}/\text{\AA}^3$ for both sizes of supercells. The numbers in the parentheses are the number of atoms in the simulation.

	Perf (512/216)	Hex (513)	Hex (217)	Tetra (513)	Tetra (217)	Vac (511)	Vac (215)
C_{11}	0.9351	0.9434	0.9556	0.9438	0.9561	0.9454	0.9587
C_{12}	0.7720	0.7771	0.7843	0.7773	0.7855	0.7792	0.7882
C_{44}	0.1631	0.1623	0.1612	0.1619	0.1619	0.1624	0.1631
\mathcal{B}	0.8264	0.8325	0.8414	0.8328	0.8423	0.8346	0.8450

We define the following brackets where v_a is the volume of the supercell:

$$[\alpha\beta, \gamma\lambda] = \frac{1}{8\pi^2 v_a} \sum_{kk'} C_{\alpha\beta, \gamma\lambda}^2(kk'), \quad (9a)$$

$$(\alpha\gamma, \beta\lambda) = -\frac{1}{4\pi^2 v_a} \sum_{kk'} \sum_{\mu\nu} \Gamma_{\mu\nu} \left\{ \sum_{k''} C_{\mu\alpha, \gamma}^1(kk'') \right\} \\ \times \left\{ \sum_{k'''} C_{\nu\beta, \lambda}^1(kk''') \right\}. \quad (9b)$$

The elastic coefficients are then

$$c_{\alpha\gamma\beta\lambda} = [\alpha\beta, \gamma\lambda] + [\beta\gamma, \alpha\lambda] - [\beta\lambda, \alpha\gamma] + (\alpha\gamma, \beta\lambda) \quad (10)$$

provided the strain energy of the crystal is invariant against rigid body rotations and the stresses on the crystal vanish. The atomistic relaxation simulation which relaxed the atoms into the lowest energy configuration and periodic boundary conditions on the supercells ensure that these conditions are satisfied.

The elastic coefficients can then be expressed in their more familiar form by pairing the indices by the equivalences $xx \rightarrow 1$, $yy \rightarrow 2$, $zz \rightarrow 3$, $yz, zy \rightarrow 4$, $xz, zx \rightarrow 5$, and $xy, yx \rightarrow 6$.

The bulk modulus \mathcal{B} (for a cubic crystal) is then

$$\mathcal{B} = \frac{C_{11} + 2C_{12}}{3}. \quad (11)$$

Table II shows the independent elastic coefficients for the various crystals in the two simulations. We calculate the entire 6×6 elastic matrix in both cases and find, as expected, that $C_{11} = C_{22} = C_{33}$, $C_{44} = C_{55} = C_{66}$, and $C_{12} = C_{21} = C_{23} = C_{32} = C_{13} = C_{31}$. All other coefficients are zero. The bulk modulus is higher than that of experiment ($\mathcal{B}=0.61 \text{ eV}/\text{\AA}^3$) because the parameters of the potential are fitted for $C = 0$, although the elastic coefficients are sensitive to the value of C . It can be seen, however, that the change in bulk modulus seems to be almost independent of the type of defect under consideration.

In comparison to experimental data²⁵ we overestimate C_{11} (for the perfect crystal) by only 1.2% which is an improvement on the SW potential where C_{11} is overestimated by 10%.²⁵ However, the covalent bond potential overestimates C_{12} by double whereas SW only overestimates by 25–30%. Like the SW potential we also underestimate the shear modulus C_{44} by a large amount although SW is closer to experiment. Neither the covalent

bond charge potential nor the SW potential were fitted to elastic constants therefore it is not unusual in that they are not in agreement with experimental results, with the exception of C_{11} where our calculation is remarkably close to that of experiment.

The elastic coefficients are also calculated for the smaller supercell, allowing us to find the change in elastic coefficients with respect to concentration. The coefficients are seen to rise with concentration (Fig. 3), apart from C_{44} which decreases very slightly. This is showing the characteristic defect stiffening in silicon.^{4,26} From these graphs we can calculate the defect strain polarizabilities which relate concentration of defect to stiffness by

$$\alpha_{ij} = \frac{\Delta C_{ij}}{c C_{ij}}, \quad (12)$$

where c is the defect concentration, ΔC_{ij} is the change in elastic coefficient caused by the defect, and C_{ij} is the elastic coefficient of the perfect crystal. The defect strain polarizabilities are shown in Table III. We find that a vacancy causes greater stiffening of the crystal than either of the interstitials.

V. STATISTICAL CALCULATIONS

Temperature dependence of thermodynamic quantities can be calculated from simulations performed at a sin-

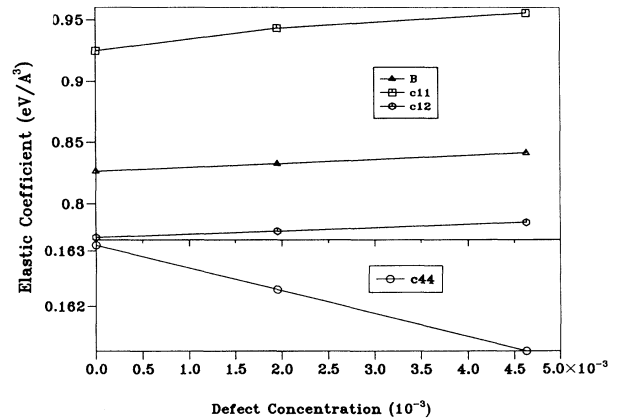


FIG. 3. Changes in elastic coefficients with respect to concentration are shown for the hexagonal interstitial. We find the changes in elastic coefficients with respect to concentration, dc_{ij}/dC , are constant. Note the change in scale for C_{44} .

TABLE III. Defect strain polarizabilities α_{ij} are shown for the various defects. It can be seen that the vacancy causes the crystal to stiffen to a greater degree than either of the self-interstitials.

	Hexagonal	Tetrahedral	Vacancy
α_{11}	4.55	4.77	5.63
α_{12}	3.39	3.52	4.76
α_{44}	-2.52	-3.77	-2.19
α_B	3.79	3.97	5.07

gle temperature.^{27,28} For example, free energy of a solid can be determined from the local atomic configuration, hence a minimization of the free energy with respect to atomic coordinates gives both the equilibrium structure and free energy of the solid which could contain defects. This requires thermal statistics to be gathered in either a MD or Monte Carlo simulation to calculate the canonical average of a thermal quantity. A series expansion of the partition function in configurational space for a thermodynamic quantity can then yield values in the surrounding phase space.

We do not do this as we already have the defect configuration and the phonon modes associated with such a configuration. Thermal properties using the vibrations within the crystal can be calculated simply from statistical mechanics. Since all of the vibrational modes are known, the partition function is calculated simply from Bose-Einstein statistics:

$$Z = \prod_{i=1}^{3N-3} \frac{1}{1 - \exp\left(\frac{-\hbar\omega_i}{k_B T}\right)}, \quad (13)$$

where i labels the $3N - 3$ nonzero vibrations allowed within the supercell. This allows us to calculate the vibrational free and ionic vibrational energies and also the vibrational entropy.

By taking the differences between the perfect crystal and the crystals containing defects (scaled to the same number of atoms) we can see the effects that the defects have on the thermal properties. The plots of these excess free energies, ionic vibrational energies, and entropies in the harmonic approximation against temperature are shown in Fig. 4. These can be compared to Fig. 5 which shows the total vibrational free energy, ionic vibrational energy, and entropy for the perfect crystal. These quantities for the defected crystals are not shown in this figure since they are indistinguishable at this scale. We find that the tetrahedral interstitial has the highest vibrational free energy at any temperature. We also note that the excess vibrational free energy within a crystal due to the defect is ~ 1000 times smaller than that of the defect formation energy and hence that the tetrahedral interstitial is stable. This leads to the conclusion that the defect formation energy for interstitials and vacancies within a crystal in the harmonic approximation is almost independent of temperature. The free energy of a silicon crystal at zero pressure was found from the SW potential by summing the logarithms of the frequencies obtained from a 512-particle dynamical matrix.²⁹ They find the

sum of the logarithms (in the reduced units of SW) to be 4.7533 per particle, although a full free energy analysis with temperature is not plotted. A similar calculation with each dynamical matrix calculated from the covalent bond charge model yields the lower value of 3.1110 for the

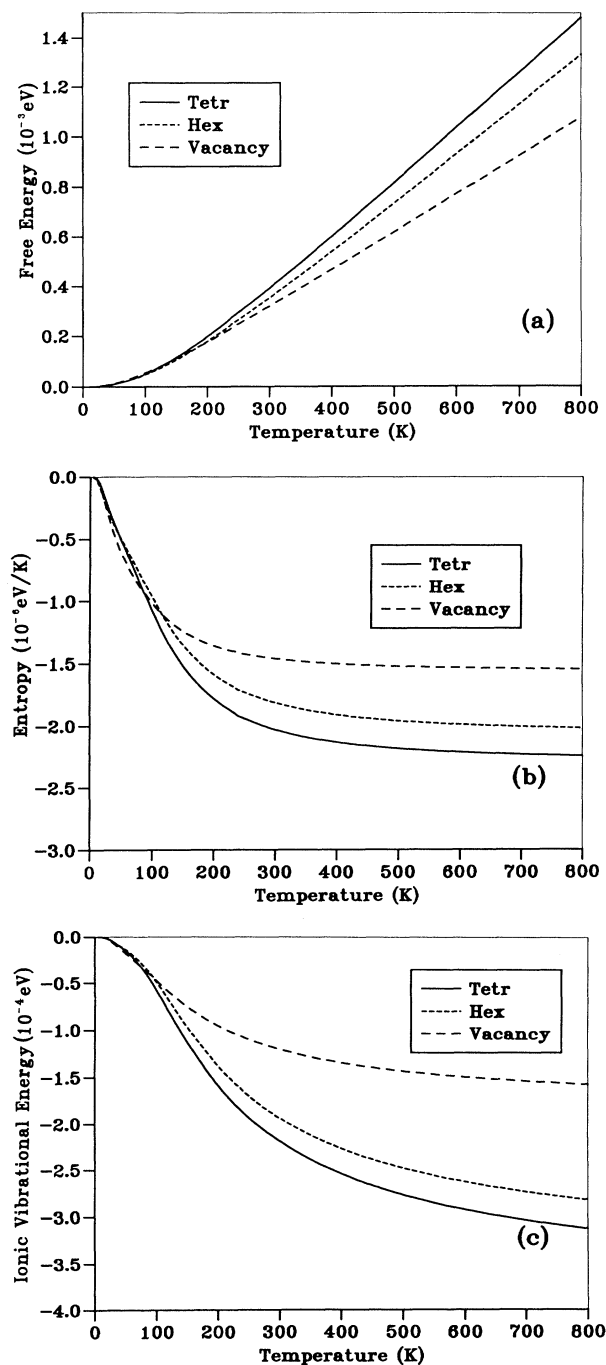


FIG. 4. Differences in (a) vibrational free energy, (b) vibrational entropy, and (c) ionic vibrational energy are shown vs temperature. The zero of each scale is taken to be the value of that property of the perfect diamond structure at each temperature.

perfect crystal. This is due to the larger density of states at the lower frequencies. The value obtained from the SW potential is expected to be larger than that of experiment since the TO bands of the dispersion relation have significantly higher frequencies than that of experiment.

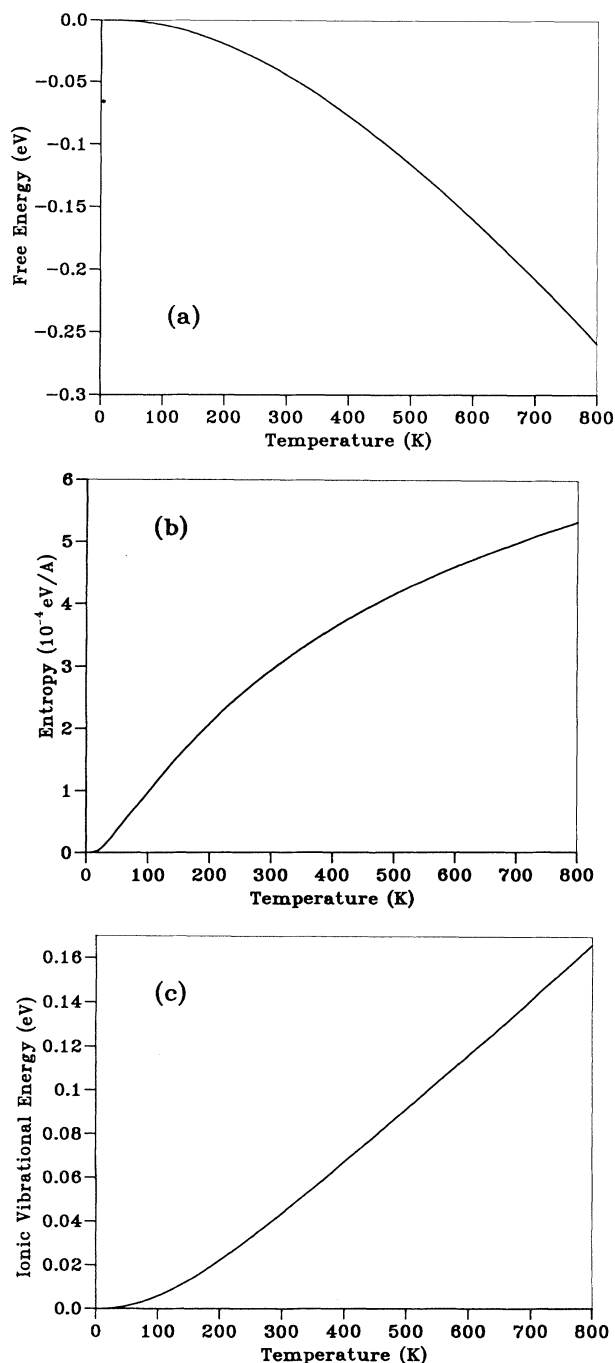


FIG. 5. Plots of ionic vibrational energy, free energy, and entropy per atom vs temperature. Only the plots for the perfect crystal are shown since the differences in the curves for the defects are too small to be seen on this scale (see Fig. 4).

Calculations on the hexagonal and tetrahedral interstitial and vacancy with the covalent model give (in SW reduced units) 3.0845, 3.0872, and 3.0928, respectively.

The defect formation energies can also be found, including the anharmonicity, by running the molecular dynamics simulation described in Sec. II, including temperature, over an extended period of time to collect thermal averages. We ran simulations comprising the perfect crystal with defect for 12 000 time steps of 1.0 fs which is longer than 10 periods of the lowest frequency vibrations (Fig. 1). This allowed us to evaluate the anharmonic defect formation energy to within 3.0%. We find that the defect formation energy is unchanged within a temperature range of 0–1000 K. This confirms the validity of obtaining our result using the harmonic approximation.

Finally, we calculate the configurational entropy of the defects to give a comparison to the vibrational entropy. The Boltzmann definition of entropy, $S = k_B \ln \Omega$, where Ω is the number of configurations, can be used to calculate the configurational entropy per atom, after simplification by Stirling's formula, by

$$S = k_B \ln \left(\frac{m}{c} \right), \quad (14)$$

where m is the number of possible different defect sites and c is the defect concentration. The configurational entropies for the three defects considered are shown in Table IV. We find that under the harmonic approximation, the contributions to the entropy of a crystal are given by the configurational entropy and vibration entropy in roughly equal proportions at nonzero temperature.

In the converged calculations the difference in interstitial formation energy between tetrahedral and hexagonal is 2.0 eV (Table I). From Fig. 5, the vibrational free energy is not enough to transform a tetrahedral interstitial to the hexagonal position. The relative stability of the anharmonic case is tested by running molecular dynamics at increasing temperature, allowing the bonding to change throughout the simulation. We do not find a transition from the tetrahedral to hexagonal site at temperatures up to 1360 K and at higher temperatures we find that the interstitial is free to move throughout the crystal. This demonstrates that the harmonic approximation we have taken is accurate up to relatively high temperatures. Recent work using the SW potential on self-interstitial diffusivity in silicon³⁰ has found a simple migration path for several self-interstitials over a temperature range of 733–1473 K. In this work the relaxation was done in a somewhat different way from our MD simulations. Energy minimization was carried out by quenching the system by a steepest descents algorithm after relaxing the system by a lengthy Monte Carlo

TABLE IV. Configurational entropies for the large and small supercells. The units are in 10^{-4} eV/K per defect.

Defect	Large supercell	Small supercell
Hexagonal interstitial	5.377	4.635
Tetrahedral interstitial	6.572	5.831
Vacancy	6.321	5.575

method at 500 K with system sizes of the host crystal ranging from 64 atoms to 512. Both calculations suggest that the tetrahedral configuration is the more stable (by 2.0 eV and 1.74 eV, respectively), but the SW formation energies are both significantly larger (by about 2 eV). However, they find that a lower symmetry extended self-interstitial has the most stable configuration of 3.66 eV. Their calculations suggest a migration mechanism of the extended interstitial where the extra atom moves from this low energy state to an identical one by passing through the state of a tetrahedral interstitial, thus requiring less energy than the tetrahedral-hexagonal transition that we have calculated above. We have not examined migration paths but concur that diffusion of the tetrahedral interstitial via a path through the hexagonal state does not occur until a much higher temperature than the Maroudas-Brown diffusion mechanism.³⁰

VI. DISCUSSION

We have carried out a complete analysis of the harmonic behavior of point defects in silicon using an empirical potential. The supercell method has allowed us to calculate the phonon densities of states and elastic constants for various point defect concentrations and compare the results by applying the same method to the perfect crystal. Knowledge of the complete densities of states also enabled us to determine the change in thermodynamic properties of the crystal caused by the defects and compare them to the configurational properties. The results lend support to the common assumption that the two quantities are interchangeable. The supercell method has also allowed us to calculate the small change in defect formation energies with respect to temperature. This result could not be obtained with comparable computational effort by running a molecular dynamics simulation and collecting thermal averages due to the short time step required in the simulation compared to the lowest frequency vibrations, our results there were only accurate enough to show the formation energies were not significantly changed.

We find that the covalent bond charge potential gives a reasonable description of many properties of point defects

in silicon, being able to predict the relative stability of the defects and their configuration. It inaccurately describes the values of some elastic coefficients, but does find that defect stiffening occurs in silicon.

Analysis of the normal modes shows that some high frequency modes are highly localized at the defect, whereas the perfect crystal has no modes closely associated with any particular atom.

The free energy of defects is dominated by the internal energy contribution, and to a first approximation the entropic and vibrational effects can be ignored. Moreover the entropy is dominated by the harmonic contribution, and again to first order anharmonic effects can be ignored. Thus we were unable to measure any anharmonic entropy effect in the free energy of formation of point defects.

This work has been made possible by applying standard lattice dynamics techniques on a large supercell using a massively parallel computer. The diagonalizations take approximately 12 min and the matrix inversions 7 min on 2¹⁴ processors. Only memory requirements prohibit larger systems from being considered since the size of the dynamical matrices is of order $(3N)^2$. A possible method of increasing the size of system and hence the complexity of the defects that could be considered is to use a large cluster of atoms without periodic boundary conditions, so that the dynamical matrices become band matrices. Although this would add the extra complication of surface modes, it would reduce the memory requirements of the problem, scaling as N with a large prefactor, and allow use of an algorithm for diagonalizing sparse matrices which is an order of N faster than the Jacobi method we used to diagonalize dense matrices.

ACKNOWLEDGMENTS

S.J.C. would like to thank SERC for financial support for this work and G.J.A. thanks BP and the Royal Society of Edinburgh for support. We have also received assistance from the Edinburgh Parallel Computing Centre on whose Connection Machine the calculations were performed.

¹P. Bruesch, in *Phonons: Theory And Experiments*, edited by M. Cardona, P. Fulde, and H. J. Queisser, Springer Series in Solid-State Science Vol. 10 (Springer-Verlag, Berlin, 1982).

²R. D. Hatcher, R. Zeller, and P. H. Dederichs, *Phys. Rev. B* **19**, 5083 (1979).

³P. W. M. Jacobs, M. A. Nerenberg, and J. Govindarajan, in *Computer Simulation in Solids*, edited by C. R. A. Catlow and W. C. Mackrodt, Lecture Notes in Physics Vol. 166 (Springer, Berlin, 1982).

⁴H. R. Schober and K. W. Ingle, *J. Phys. F* **10**, 575 (1980).

⁵M. J. Gillan, J. H. Harding, and M. Leslie, *J. Phys. C* **21**, 5465 (1988).

⁶U. Scherz, S. Biernacki, J. Schopp, and D. Weider, *Z. Phys. B* **85**, 69 (1991).

⁷J. H. Harding and A. M. Stoneham, *Philos. Mag.* **43**, 705 (1981).

⁸G. J. Ackland, *Phys. Rev. B* **44**, 3900 (1991).

⁹F. H. Stillinger and T. A. Weber, *Phys. Rev. B* **31**, 5262 (1985).

¹⁰R. Biswas and D. R. Hamann, *Phys. Rev. Lett* **55**, 2001 (1985).

¹¹H. Balamane, T. Halicioglu, and W. A. Tiller, *Phys. Rev. B* **46**, 2250 (1992).

¹²S. J. Clark, G. J. Ackland, and J. Crain (unpublished).

¹³J. Crain, S. J. Clark, G. J. Ackland, M. C. Payne, V. Milman, P. D. Hatton, and B. J. Reid (unpublished).

¹⁴G. J. Ackland, *Phys. Rev. B* **40**, 10351 (1989).

¹⁵G. J. Ackland, D. Phil. thesis, Oxford, 1987.

¹⁶D. J. Chadi, *Phys. Rev. B* **46**, 9400 (1992).

- ¹⁷M. Parrinello and A. Rahman, *J. Appl. Phys.* **52**, 7182 (1981).
- ¹⁸I. P. Batra, F. F. Abraham, and S. Ciraci, *Phys. Rev. B* **35**, 9552 (1987).
- ¹⁹P. J. Kelly and R. Car, *Phys. Rev. B* **45**, 6543 (1992).
- ²⁰M. Born and K. Huang, *Dynamical Theory of Crystal Lattices* (Oxford University Press, London, 1956).
- ²¹H. Bilz and W. Kress, in *Phonon Dispersion Relations in Insulators*, edited by M. Cardona, P. Fulde, and H. J. Queisser, Springer Series in Solid-State Science Vol. 10 (Springer-Verlag, Berlin, 1979).
- ²²G. P. Srivastava and K. Kunc, *J. Phys. C* **21**, 5087 (1988), Equation 16.
- ²³P. N. Keating, *Phys. Rev.* **145**, 637 (1966).
- ²⁴A. A. Maradudin, E. W. Montroll, and G. H. Weiss, in *Theory of Lattice Dynamics in the Harmonic Approximation*, edited by H. Ehrenreich (Academic, New York, 1971), Suppl. 3.
- ²⁵M. D. Kluge, J. R. Ray, and A. Rahman, *J. Chem. Phys.* **85**, 4028 (1986).
- ²⁶H. R. Schober and K. W. Ingle, *J. Nucl. Mater.* **69/70**, 341 (1978).
- ²⁷R. LeSar, R. Najafabadi, and D. J. Srolovitz, *Phys. Rev. Lett.* **63**, 624 (1989).
- ²⁸J. M. Rickman and S. R. Phillpot, *Phys. Rev. Lett.* **66**, 349 (1992).
- ²⁹J. Q. Broughton and X. P. Li, *Phys. Rev. B* **35**, 9120 (1987).
- ³⁰D. Maroudas and R. A. Brown, *Appl. Phys. Lett.* **62**, 172 (1993).